Using EO-1 Hyperion to Simulate HyspIRI Products for a Coniferous Forest: The Fraction of PAR Absorbed by Chlorophyll ($\mathrm{fAPAR_{chl}}$) and Leaf Water Content (LWC)

Qingyuan Zhang, Elizabeth M. Middleton, *Member, IEEE*, Bo-Cai Gao, and Yen-Ben Cheng

***Abstract*—This paper presents development of prototype products for terrestrial ecosystems in preparation for the future imaging spectrometer planned for the Hyperspectral Infrared Imager (HyspIRI) mission. We present a successful demonstration example in a coniferous forest of two product prototypes: fraction of photosynthetically active radiation (PAR) absorbed by chlorophyll of a canopy ($\mathrm{fAPAR_{chl}}$) and leaf water content (LWC), for future HyspIRI implementation at 60-m spatial resolution. For this, we used existing 30-m resolution imaging spectrometer data available from the Earth Observing One (EO-1) Hyperion satellite to simulate and prototype the level one radiometrically corrected radiance (L1R) images expected from the HyspIRI visible through shortwave infrared spectrometer. The HyspIRI-like images were atmospherically corrected to obtain surface reflectance and spectrally resampled to produce 60-m reflectance images for wavelength regions that were comparable to all seven of the MODerate resolution Imaging Spectroradiometer (MODIS) land bands. Thus, we developed MODIS-like surface reflectance in seven spectral bands at the HyspIRI-like spatial scale, which was utilized to derive $\mathrm{fAPAR_{chl}}$ and LWC with a coupled canopy-leaf radiative transfer model (PROSAIL2) for the coniferous forest. With this paper, we provide additional evidence that the $\mathrm{fAPAR_{chl}}$ product is more realistic in describing the physiologically active canopy than the traditional fAPAR parameter for the whole canopy ($\mathrm{fAPAR_{canopy}}$), and thus, it should replace it in ecosystem process models to reduce uncertainties in terrestrial carbon cycle and ecosystem studies.**

Manuscript received September 2, 2010; revised January 22, 2011, April 27, 2011, and August 25, 2011; accepted September 11, 2011. Date of publication November 3, 2011; date of current version April 18, 2012. This work was supported by two NASA Headquarters sponsored programs, the Earth Observing One (EO-1) Mission Science Office (Sponsor, Garik Gutman), and the HyspIRI science support project at the Goddard Space Flight Center (NASA/GSFC) through William (Woody) Turner.

Q. Zhang is with the Goddard Earth Sciences Technology and Research (GESTAR), Universities Space Research Association (USRA), Columbia, MD 21044 USA, and also with the Biospheric Sciences Branch, NASA Goddard Space Flight Center, Greenbelt, MD 20771 USA (e-mail: qyz72@yahoo.com).

E. M. Middleton is with the Biospheric Sciences Branch, NASA Goddard Space Flight Center, Greenbelt, MD 20771 USA (e-mail: elizabeth.m.middleton@nasa.gov).

B.-C. Gao is with the Remote Sensing Division, Naval Research Laboratory, Washington, DC 20375 USA (e-mail: bo-cai.gao@nrl.navy.mil).

Y.-B. Cheng is with the Earth Resources Technology, Inc., Annapolis Junction, MD 20701 USA, and also with the Biospheric Sciences Branch, NASA Goddard Space Flight Center, Greenbelt, MD 20771 USA (e-mail: yen-ben.cheng-1@nasa.gov).

Color versions of one or more of the figures in this paper are available online at http://ieeexplore.ieee.org.

Digital Object Identifier 10.1109/TGRS.2011.2169267

***Index Terms*—Earth Observing One (EO-1) Hyperion, $\mathrm{fAPAR_{canopy}}$, $\mathrm{fAPAR_{chl}}$, foliar moisture content, Hyperspectral Infrared Imager (HyspIRI), leaf water content (LWC), terrestrial carbon cycle.**

I. Introduction

THE HYPERSPECTRAL Infrared Imager (HyspIRI) mission was described by the National Research Council in its Decadal Survey Report (http://www.nap.edu/catalog.php?record_id=11820) to address terrestrial ecosystem science as one of the next-generation NASA satellite missions. The HyspIRI mission is envisioned to carry two spectral instruments, both with ground spatial resolutions of 60 m—a visible to shortwave infrared (VSWIR) continuous spectrum hyperspectral imager (10-nm spectral sampling) and a multichannel thermal infrared (TIR) imager. The Earth Observing One (EO-1) Hyperion (launched in November 2000) is still operating and serves as the heritage satellite instrument for HyspIRI's VSWIR spectrometer, but it only captures 7.5-km-wide ground strips, and its 30-m resolution images are acquired through user/system requests. In contrast, HyspIRI will be a global survey mission, and its VSWIR instrument will have 60-m pixels across a 150-km-wide ground swath, collected on an equatorial 19-day repeat cycle. Consequently, existing Hyperion data provide an excellent tool for product development in anticipation of the HyspIRI and other spaceborne imaging spectrometer missions.

The absorbed photosynthetically active radiation (APAR) fraction for a whole vegetation canopy ($\mathrm{fAPAR_{canopy}}$, also denoted as FAPAR or FPAR [1]–[3]; see Appendix A for equations) is an essential climate variable [4]–[7] needed to estimate and monitor vegetation productivity on a global basis. However, $\mathrm{fAPAR_{canopy}}$ includes both photosynthetic and nonphotosynthetic components and has not provided consistent relationships to photosynthetic processes at the ecosystem scale [8]–[11]. This is because the APAR available to support vegetation photosynthesis ($\mathrm{APAR_{PSN}}$) is typically overestimated by $\mathrm{fAPAR_{canopy}}$. However, the APAR fraction associated with the chlorophyll-containing component ($\mathrm{fAPAR_{chl}}$, (A3) in Appendix A) consistently and correctly represents the physiologically active photosynthetic sector of the canopy under optimal (e.g., fully green) and less optimal (e.g., mixtures of green and senescent vegetation) conditions

0196-2892/$26.00 © 2011 IEEE

affecting physiological responses. In other words, $\mathrm{fAPAR_{PSN}} = \mathrm{fAPAR_{chl}}$ [11].

We recently demonstrated that $\mathrm{fAPAR_{chl}}$ is superior to the use of $\mathrm{fAPAR_{canopy}}$ in model simulations with gross primary production (GPP) or gross ecosystem production to estimate light use efficiency (LUE), defined as $\mathrm{GPP/APAR_{PSN}}$ [11]. The $\mathrm{fAPAR_{chl}}$ retrievals were estimated from space for a deciduous aspen forest using five of the seven MODerate Resolution Imaging Spectroradiometer (MODIS) spectral land bands from Collection 4 daily products, for which product quality was insufficient for our model retrievals in two land bands (B3, blue; B7, $\mathrm{SWIR_2}$). Those earlier results were indirectly validated by comparing LUE measured *in situ* at the tower $(\mathrm{LUE_{tower}})$ to the LUE determined from our remote sensing/modeling approach for the forest's chlorophyll component ($\mathrm{LUE_{chl}} = \mathrm{GPP/APAR_{chl}}$, where $\mathrm{APAR_{chl}} = \mathrm{fAPAR_{chl}} * \mathrm{PAR}$). $\mathrm{LUE_{chl}}$ matched well with $\mathrm{LUE_{tower}}$, while the widely used LUE describing the whole canopy ($\mathrm{LUE_{canopy}} = \mathrm{GPP/APAR_{canopy}}$, where $\mathrm{APAR_{canopy}} = \mathrm{fAPAR_{canopy}} * \mathrm{PAR}$) did not. Therefore, we recommended that $\mathrm{fAPAR_{chl}}$ should replace $\mathrm{fAPAR_{canopy}}$ to estimate canopy parameters related to photosynthesis for climate models and land–atmosphere interaction models [4], [6]. However, further evidence should be pursued.

The spectral range for both the EO-1 Hyperion and future HyspIRI VSWIR imaging spectrometers is between 0.4 and 2.5 μm, which spans the spectral range of the MODIS 1–7 land bands. In the present study, the $\mathrm{fAPAR_{chl}}$ algorithm that was previously developed to ingest five MODIS bands was modified to utilize all seven MODIS land bands from the more radiometrically rigorous Collection 5 products. We wish to know how inclusion of these additional bands and higher spatial resolution satellite observations (60 versus 500 m) affected and improved retrievals of $\mathrm{fAPAR_{chl}}$ from HyspIRI-like VSWIR radiance images simulated from EO-1 Hyperion images. We also simultaneously retrieved leaf water content [LWC, (A4)]. The Normalized Difference Vegetation Index [NDVI, (A5)] and Enhanced Vegetation Index [EVI, (A6)] were used to estimate $\mathrm{fAPAR_{canopy}}$ and $\mathrm{fAPAR_{chl}}$, respectively [12]–[15], and the Land Surface Water Index [LSWI, (A7)] was used to estimate foliar moisture content [14]. Note that $\mathrm{fAPAR_{canopy}}$ is a linear function of NDVI [12].

The goal of this paper was to apply the modified $\mathrm{fAPAR_{chl}}$ and LWC algorithm to a coniferous forest in a heterogeneous landscape, to demonstrate the advantages of the revised algorithm to observations with spectral bands spanning the full optical spectrum at much high spatial resolution than is possible with MODIS. Our specific objectives were to test the following hypotheses: 1) $\mathrm{fAPAR_{chl}}$ and LWC provide unique information, as compared to existing indices such as EVI, $\mathrm{fAPAR_{canopy}}$ (linear function of NDVI), and LSWI, and 2) $\mathrm{fAPAR_{chl}}$ and LWC retrievals benefit from higher spatial resolution and additional spectral band inputs. We begin by describing the approach to obtaining prototype HyspIRI VSWIR radiance images and then describe the modification of the $\mathrm{fAPAR_{chl}}$-LWC algorithm from five- to seven-band versions. Next, we present the HyspIRI outputs of the seven-band algorithm and comparisons of our model retrievals for 500- versus 60-m pixels, and comparison of 500-m retrievals using five versus seven spectral bands, followed by the summary conclusion.

II. Methods

A. Satellite Image Preprocessing

1) Spatially Scaling Up the EO-1 Hyperion Radiance Images to 60 m: The EO-1 Hyperion images have a spatial resolution of 30 m. We spatially scaled up the Hyperion Level One radiometrically corrected Radiance (L1R) data to 60 m by averaging Hyperion 30-m pixels in four-pixel blocks [16], [17] to obtain a spatially relevant prototype of 60-m HyspIRI L1R data, also achieving an average signal to noise response comparable to that expected for HyspIRI ($\geq 400:1$). These measured radiances were divided by solar irradiances above the atmosphere to obtain the apparent top-of-atmosphere (TOA) reflectances.

2) Atmospheric Correction With the ATREM Routine: In order to use spectral imaging data for quantitative remote sensing of land surfaces, the absorption and scattering effects of atmospheric gases and aerosols must be removed [18]. The HyspIRI-like L1R images (at 60 m) were atmospherically corrected using an updated version of the ATmosphere REMoval Algorithm (ATREM) with which a line-by-line model was used to calculate atmospheric gaseous transmittances [19], [20]. The surface reflectances were derived from the apparent TOA reflectances using the simulated atmospheric gaseous transmittances and the simulated molecular and aerosol scattering data. During retrievals, the integrated water vapor amount on a pixel-by-pixel basis can be directly derived from the 0.94- and the 1.14-μm atmospheric water vapor absorption features, a special advantage conveyed by continuous spectrometer data. The transmission spectrum of water vapor $(\mathrm{H_2O})$, carbon dioxide $(\mathrm{CO_2})$, ozone $(\mathrm{O_3})$, nitrous oxide $(\mathrm{N_2O})$, carbon monoxide (CO), methane $(\mathrm{CH_4})$, and oxygen $(\mathrm{O_2})$ in the 0.4–2.5-μm region was simulated based on the derived water vapor value and the solar and observational geometry, and through the use of narrowband spectral models. However, the scattering effect due to atmospheric molecules and aerosols was determined with the 6S computer code [21].

3) Spectrally Combining HyspIRI-Like Surface Reflectance Bands to Simulate the MODIS Bands 1–7: After obtaining atmospherically corrected HyspIRI-like 60-m surface reflectance images, the spectral values were averaged across 3–6 contiguous 10-nm Hyperion bands within the defined MODIS band ranges (Table I) using spectral response functions to obtain reflectances spectrally comparable to those from MODIS [22]. This yielded an image that was spatially HyspIRI-like but spectrally MODIS-like. To summarize, spatially scaling-up from 30 to 60 m was performed on the Hyperion L1R radiance image; after which, the ATREM atmospheric correction was performed on the 60-m HyspIRI-like L1R radiance image (60×60 HyspIRI pixel block) to obtain a 60-m HyspIRI-like surface reflectance image, followed by spectral averaging to obtain surface reflectance in each of the seven MODIS-like bands (Table I).

The vegetation canopy parameters derived from the $\mathrm{fAPAR_{chl}}$ algorithm [11] included the following: leaf internal structure (N), leaf dry matter $(\mathrm{C_m})$, leaf water thickness $(\mathrm{C_w})$, and leaf pigment content $(\mathrm{C_{ab}})$. In preliminary model runs, all seven (of 36) MODIS land bands (1–7) were found to be sensitive to N and $\mathrm{C_m}$, whereas bands 1, 3, and 4 were sensitive to $\mathrm{C_{ab}}$, and bands 5, 6, and 7 were sensitive to $\mathrm{C_w}$ [23].

TABLE I
SPECTRAL RANGES COVERED BY THE MODIS AND HYPERION/HYSPIRI BANDS

Spectral range/ Band Width	MODIS band #	Hyperion/HyspIRI band #
459 – 479 nm/ 20 nm	3 (blue)	11 – 13
545 – 565 nm/ 20 nm	4 (green)	20 – 22
620 – 670 nm/ 50 nm	1 (red)	27 – 32
841 – 875 nm/ 34 nm	2 (NIR_1)	49 – 52
1230 – 1250 nm/ 20 nm	5 (NIR_2)	108 – 111
1628 – 1652 nm/ 24 nm	6 ($SWIR_1$)	148 – 150
2105 – 2155 nm/ 50 nm	7 ($SWIR_2$)	195 – 200

B. Algorithm to Derive $fAPAR_{chl}$ and LWC Using PROSAIL2 and the Metropolis Approach

A complete description of the PROSAIL2 model and Metropolis approach, as applied to five spectral MODIS land bands, is given in a recent publication [11]. The coupled canopy-leaf radiative transfer model utilized in this PROSAIL2 algorithm is based on the SAIL2 canopy radiative transfer model and the PROSPECT leaf radiative transfer model. Here, we provide an overview and highlight the changes introduced in the revised approach. Additional details and information are provided in Appendix A.

In brief, a vegetation canopy can be partitioned into leaf and nonleaf (referred to as stem) components. A leaf can be further partitioned into chlorophyll, nonphotosynthetic pigments (referred to as brown pigment C_{brown}), water, and dry matter. The PROSAIL2 model has 14 biophysical and biochemical variables (see Appendix A), including five leaf variables that simulate leaf optical properties (N, C_{ab}, C_m, C_w, and C_{brown}), a soil/litter variable that simulates soil/litter optical properties ($SOIL_A$), and a variable that simulates stem optical properties ($STEM_A$).

We modified the previous MODIS $fAPAR_{chl}$ algorithm [11] by replacing the five-band likelihood function with that for seven-band surface reflectances obtained from Section II-A3 [(1) and (2)]. The Markov Chain Monte Carlo (MCMC) method (Metropolis) is employed for inversion. This method assumes that the observed spectral reflectances $X_i = [x_{i1}, \ldots, x_{ip}]'$ ($p = 7$; Table I) differ from the model predicted values $U_i = [u_{i1}, \ldots, u_{ip}]'$ according to a mean zero p-variate Gaussian error model that results in the likelihood function

$$L = \prod_{i=1}^{n} \frac{1}{(\sqrt{2\pi})^p |\Sigma|^{\frac{1}{2}}} e^{-(X_i - U_i)' \Sigma^{-1} (X_i - U_i)/2} \quad (1)$$

where n is the number of data points sampled according to equation (8) of Zhang *et al.* [11] and Σ is the variance–covariance matrix of X

$$\sum_e = (s_{ij})_{p \times p}$$

$$s_{ij} = \frac{1}{n} \sum_{k=1}^{n} (x_{ki} - u_{ki})(x_{kj} - u_{kj}), \qquad i, j = 1, \ldots, p. \quad (2)$$

The new seven-band $fAPAR_{chl}$ algorithm provides simultaneous solutions for C_w and C_m, enabling the solution of LWC [see (A4)]. The full solution of the 14 parameters is a statistical posterior distribution based on the radiative transfer model and the remote sensing observation (see Section II-A3).

The 14 parameters and the derived $fAPAR_{chl}$ and LWC may be grouped into three classes based on their posterior statistical distributions: well-constrained, edge-hitting, and poorly constrained. The posterior statistical distributions can provide the mode(s) of the 14 variables, $fAPAR_{chl}$, and LWC (if they exist) (please see Zhang *et al.* [24] for details). A mode for a variable is one "traditional" (best) point solution, i.e., the most likely value of the variable to fit both the PROSAIL2 model and the remote sensing observation. From the case study of this paper (see Section II-C for site description), we discovered that there was one and only one mode for $fAPAR_{chl}$ and for LWC per satellite observation. The reason is that chlorophyll, leaf water, and dry matter have unique spectral characteristics. These components can be distinguished using spectral information of the seven bands, and they will not mess up with each other or other components of a canopy.

The EVI [25], NDVI [26], $fAPAR_{canopy}$, and LSWI [14] were also calculated (see Appendix for equations) and compared with results for $fAPAR_{chl}$ or LWC, as appropriate, at both MODIS (500 m) and HyspIRI (60 m) spatial resolutions. We also calculated $fAPAR_{canopy}$ for the whole canopy based on a widely used formula which relates $fAPAR_{canopy}$ and NDVI (e.g., [12], [13], and [15])

$$fAPAR_{canopy} = 1.24 \times NDVI - 0.168. \quad (3)$$

We also utilized the same seven-band approach [(1) and (2)] to retrieve $fAPAR_{chl}$ and LWC from MOD09A1 [the eight-day composite reflectance MODIS product (M)] acquired on day 185 (July 3, 2008), which was close to the acquisition date of the original Hyperion image (June 28, 2008). This enabled us to compare the 60-m HyspIRI-like product (H) with MODIS 500-m product.

C. Study Site

The study site (Fig. 1) was a Douglas fir forest surrounding an instrumented tower (hereafter DF49: 49° 52′ N, 125° 20′ W, 300-m elevation) in the Canadian Carbon Program network. The DF49 is located at the eastern side of Vancouver Island, BC, Canada, and the forest stand around the tower (indicated by a circle in Fig. 1) is mainly comprised of Douglas fir with some western red cedar and western hemlock [27]. The study area was a 120 × 120 grid formed by Hyperion pixels at the original 30-m spatial resolution around the DF49 site. A true color red/green/blue (RGB) image at the 60-m HyspIRI pixel spatial resolution (Fig. 1) can be compared with the land cover map produced using the ISODATA method of ENVI (Fig. 2), which utilized the surface reflectances of the original HyspIRI bands (Table I) for land cover classification. "Unvegetated" areas are associated with roads or sparse vegetation. Harvested areas show various stages of forest regeneration. Wetter forested areas are dominated by hemlock, alder, and maple (personal communication, Nicholas Coops, University of British Columbia, Vancouver, BC, Canada).

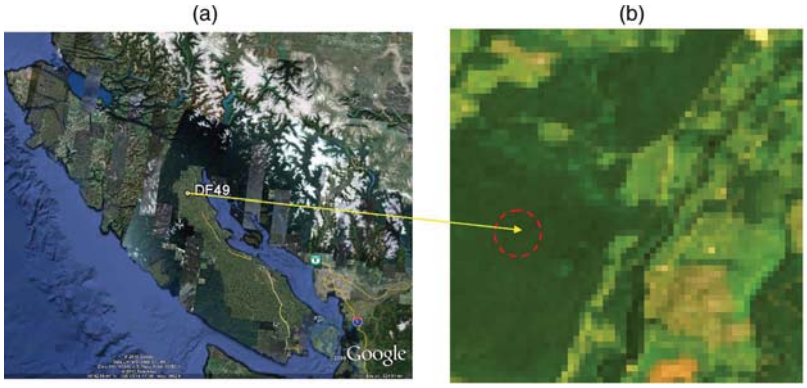

Fig. 1. (a) Location of the Douglas fir site (DF49) on Vancouver Island, BC, Canada. (b) True color RGB image for the DF49 area using simulated HyspIRI data on DOY 180, 2008 (June 28, 2008), where the circle designates the fetch of the DF49 flux tower.

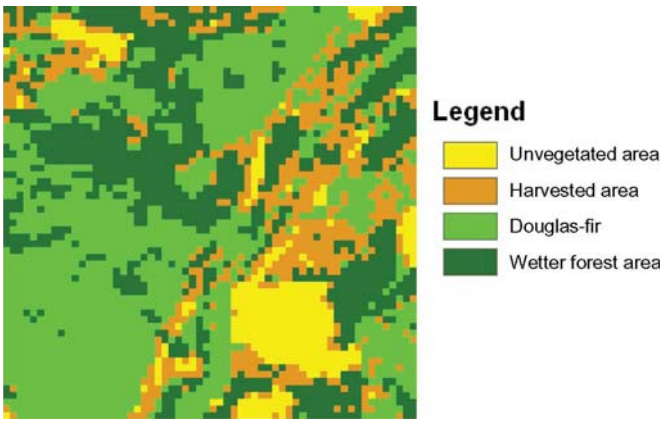

Fig. 2. Land cover map for the DF49 area using simulated HyspIRI data based on the EO-1 Hyperion image collected on DOY 180, 2008 (June 28, 2008).

III. Results

A. HyspIRI-Like Results

Here, we present the results of the revised seven-band $\mathrm{fAPAR_{chl}}$-LWC algorithm (described in Section II-B) applied to the mid-summer HyspIRI-like L1R radiance image in the vicinity of the DF49 Douglas fir tower site (described in Section II-C) for the purpose of developing and evaluating prototype products.

Fig. 3 has three subfigures for our study site showing the spatial distributions for three of the variables of interest: 1) $\mathrm{fAPAR_{chl}}$; 2) $\mathrm{fAPAR_{canopy}}$ [based on NDVI using (3)]; and 3) EVI, all presented on the same relative scale between 0.0 and 1.0. Clearly, the values in the $\mathrm{fAPAR_{chl}}$ map are substantially and statistically lower than those exhibited by the $\mathrm{fAPAR_{canopy}}$ map. Table II lists the mode, mean, and median values computed for the study area shown in Figs. 1(b), 2, and 3(a)–(c) for $\mathrm{fAPAR_{chl}}$, EVI, $\mathrm{fAPAR_{canopy}}$, and NDVI. These statistical values reveal that $\mathrm{fAPAR_{chl}}$ and EVI provide substantially lower values than NDVI and $\mathrm{fAPAR_{canopy}}$.

The vegetation photosynthesis model (VPM) [14] assumes $\mathrm{fAPAR_{chl}} = \mathrm{EVI}$, but we find that this assumption is not always correct. Moreover, overestimates of $\mathrm{APAR_{PSN}}$ result if we assume $\mathrm{fAPAR_{chl}} = \mathrm{fAPAR_{canopy}}$.

The LWC and LSWI maps are shown in Fig. 4. The LWC values of wetter forest areas (0.600–0.909) differ substantially from LSWI values (0.202–0.483). Although the LSWI has been shown to represent water status of vegetation in some studies [14], [28], this index cannot distinguish canopy water from background water (e.g., soil water). The LWC of different plant species among land cover types might vary, as shown in Fig. 4(a) for the LWC dynamics per class. The broad-leaf deciduous leaves in the wetter forest areas had higher average LWC than the Douglas fir leaves [Fig. 4(a)].

The histograms for $\mathrm{fAPAR_{chl}}$, $\mathrm{fAPAR_{canopy}}$, and EVI and the histograms for LWC and LSWI are shown in Figs. 5 and 6, respectively. Peak frequencies occurred at very different values: $\mathrm{fAPAR_{chl}}$ (0.559), EVI (0.437), and $\mathrm{fAPAR_{canopy}}$ (0.893), but peak frequencies for LWC and LSWI occurred at similar value ($\sim$0.49). The $\mathrm{fAPAR_{chl}}$ parameter displayed minor mode at 0.714. For forests, the magnitude is higher, and the range is wider for $\mathrm{fAPAR_{chl}}$ as compared to EVI [Fig. 3(a) and (c)]. The frequency of the mode derived from the HyspIRI-like LWC map is about three times that of the comparable mode for the LSWI (Fig. 6). Scatter plot comparisons are also shown for these pairs: $\mathrm{fAPAR_{chl}}$ versus $\mathrm{fAPAR_{canopy}}$, $\mathrm{fAPAR_{chl}}$ versus EVI, and LWC versus LSWI (Fig. 7). The first pair exhibits that $\mathrm{fAPAR_{canopy}}$ is greater than $\mathrm{fAPAR_{chl}}$. While values are closer between EVI and $\mathrm{fAPAR_{chl}}$, the slope relating these two variables clearly deviates from the 1:1 line. No apparent correlation is seen for the third pair (LWC and LSWI). LSWI cannot be used to replace or predict LWC well, as shown in Fig. 7(c).

The pixels classified as "unvegetated" were recently harvested (personal communication, Nicholas Coops, University of British Columbia). The $\mathrm{fAPAR_{chl}}$ values for those pixels are close to zero, as should be expected for areas without green vegetation. That is to say that $\mathrm{fAPAR_{chl}}$ has a physical and physiological meaning. However, the NDVI and EVI values of those pixels, which are greater than 0.4 and 0.2, respectively, indicate the presence of some green vegetation. NDVI (and the derived parameter $\mathrm{fAPAR_{canopy}}$) saturates for pixels with a leaf area index greater than three [25], while $\mathrm{fAPAR_{chl}}$ does not.

B. Comparing HyspIRI-Like and MODIS Parameter Estimates

From the processed MODIS image (July 3, 2008; DOY 185), we selected the pixel that covers the DF49 site. The HyspIRI-like maps have considerably more spatial details than those

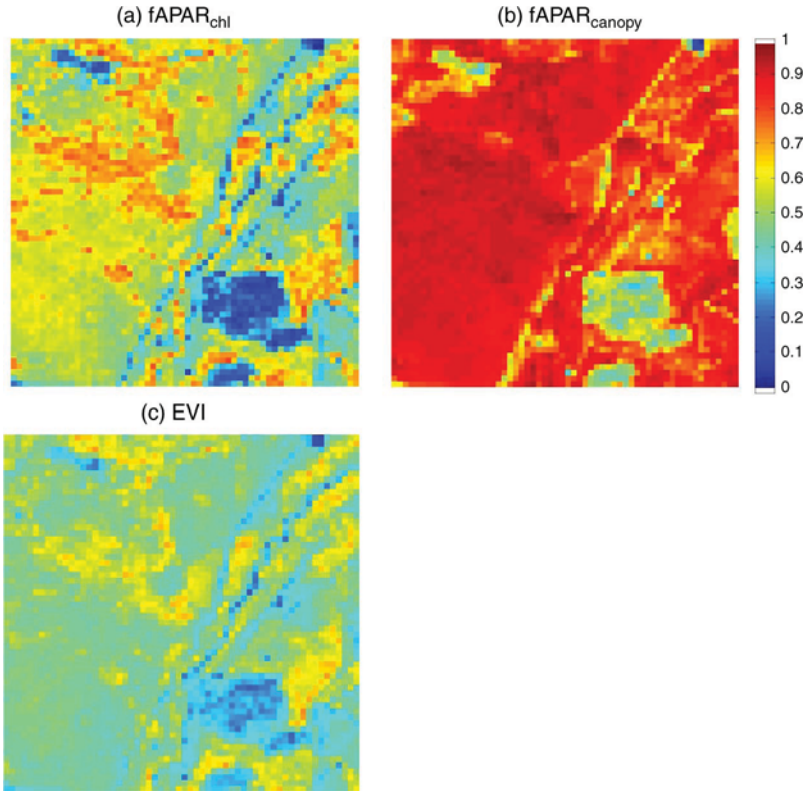

Fig. 3. HyspIRI-like maps for the DF49 area. (a) fAPAR$_{\rm chl}$. (b) fAPAR$_{\rm canopy}$ computed from NDVI (3). (c) EVI. Data were simulated from the mid-summer Hyperion image acquired on DOY 180, 2008 (June 28, 2008).

TABLE II
VALUES OF MODE(S), MEAN, AND MEDIAN OF THE $fAPAR_{\rm chl}$, EVI, $fAPAR_{\rm canopy}$, AND NDVI VALUES FOR THE AREA SHOWN IN FIG. 3. NUMBER OF HYSPIRI-LIKE $Pixels = 3600$

	mode(s)	mean	median
fAPAR$_{chl}$	0.559, 0.714	0.520	0.544
EVI	0.437	0.460	0.452
fAPAR$_{canopy}$	0.893	0.824	0.870
NDVI **	0.855	0.800	0.837

** map not shown.

based on the MODIS image. To compare our retrievals from HyspIRI-like images with those based on the MODIS image, using the same seven-band approach [(1) and (2)], we chose only the HyspIRI pixels that fall within 240 m of the DF49 tower site. Forty-nine HyspIRI pixels were selected (Table III).

In the comparison of the seven-band HyspIRI-like (H) and true MODIS (M) products (Table III), the mean fAPAR$_{\rm chl}$ values (H) and the single MODIS fAPAR$_{\rm chl}$ value (M) were fairly similar. The mean H and M satellite values for fAPAR$_{\rm canopy}$ were comparable to the tower-based canopy-level fAPAR (0.94 [29]) determined from the DF49 tower radiation measurements for the same period. The green leaf fAPAR (0.79 [30]) estimated using the approach developed by Chen *et al.* [31], [32] represented the combined effects of chlorophyll fAPAR and the fAPAR of leaf dry matter and brown pigments of the canopy for the same period. Thus, the green leaf fAPAR was intermediate between estimates for fAPAR$_{\rm chl}$ and fAPAR$_{\rm canopy}$.

LWC provides quantitative information on foliar moisture content. It is not only a critical indicator of vegetation growth status but also an important factor in the canopy susceptibility to the fire ignition process. Our LWC retrievals for H and M (Table III) both fall within the published Douglas fir LWC range (between 0.67 and 0.44), which includes both young and old leaves [33], [34]. The mean LWC value for the 49 HyspIRI-like pixels [Fig. 4(a)] is the same as that for the MODIS single pixel LWC ($\sim$0.49; Table III).

In addition to application of the seven-band algorithm to the MODIS pixel that covers the DF49 site, we also calculated fAPAR$_{\rm chl}$ and LWC using the original five-band algorithm [11]. The seven-band versus five-band fAPAR$_{\rm chl}$ histograms of the pixel have the same mode value (0.533), with only slightly different standard deviations (0.071 versus 0.072). However, while the seven-band versus five-band LWC histograms at the tower site have the same mode value, their standard deviations differ (0.169 versus 0.174), such that less uncertainty is incurred using the seven-band version.

IV. DISCUSSION

This paper describes how to estimate two products (fAPAR$_{\rm chl}$ and LWC) for HyspIRI L1R radiance and presents some initial prototype results. In addition to our primary products (fAPAR$_{\rm chl}$ and LWC), we also determined values and map products for the EVI, fAPAR$_{\rm canopy}$, and LSWI. Although fAPAR$_{\rm chl}$ and EVI were the most similar, the range of values and the modes for fAPAR$_{\rm chl}$ were larger than those obtained for the EVI (Fig. 5(a) and (c); Table II). Likewise, the dynamic range for fAPAR$_{\rm canopy}$ was smaller than the range

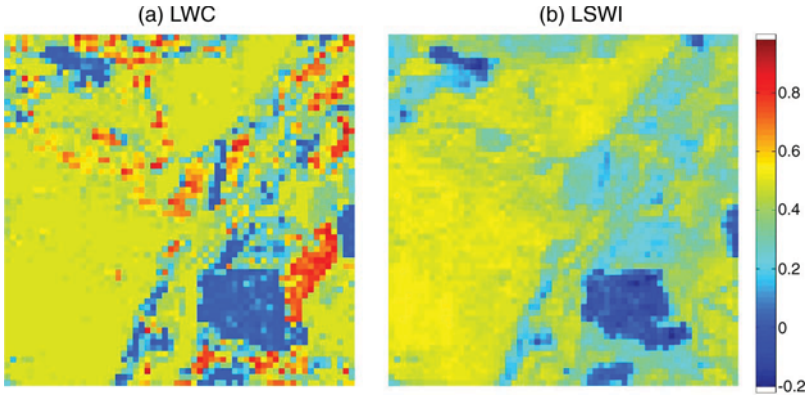

Fig. 4. HyspIRI-like maps for the DF49 area. (a) LWC. (b) LSWI. Data were simulated from the mid-summer Hyperion image acquired on DOY 180, 2008 (June 28, 2008).

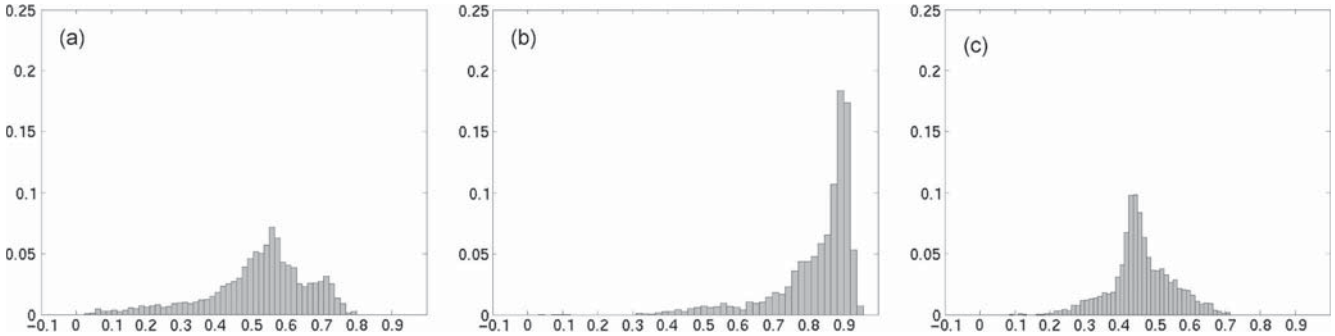

Fig. 5. Histograms for (a) $\mathrm{fAPAR_{chl}}$, (b) $\mathrm{fAPAR_{canopy}}$, and (c) EVI for the DF49 area shown in the Fig. 3 maps.

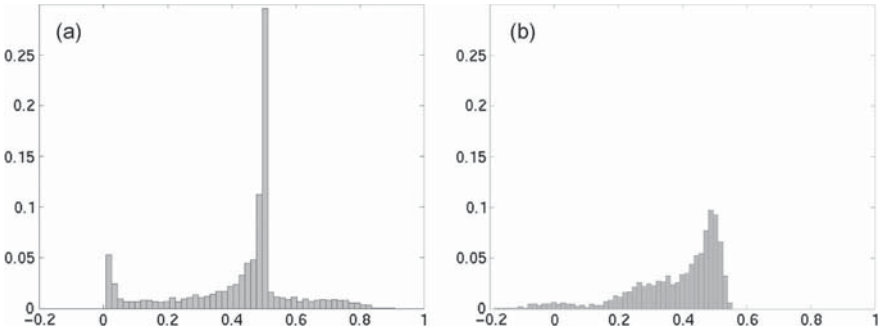

Fig. 6. Histograms for (a) LWC and (b) LSWI for the DF49 area shown in the Fig. 4 maps.

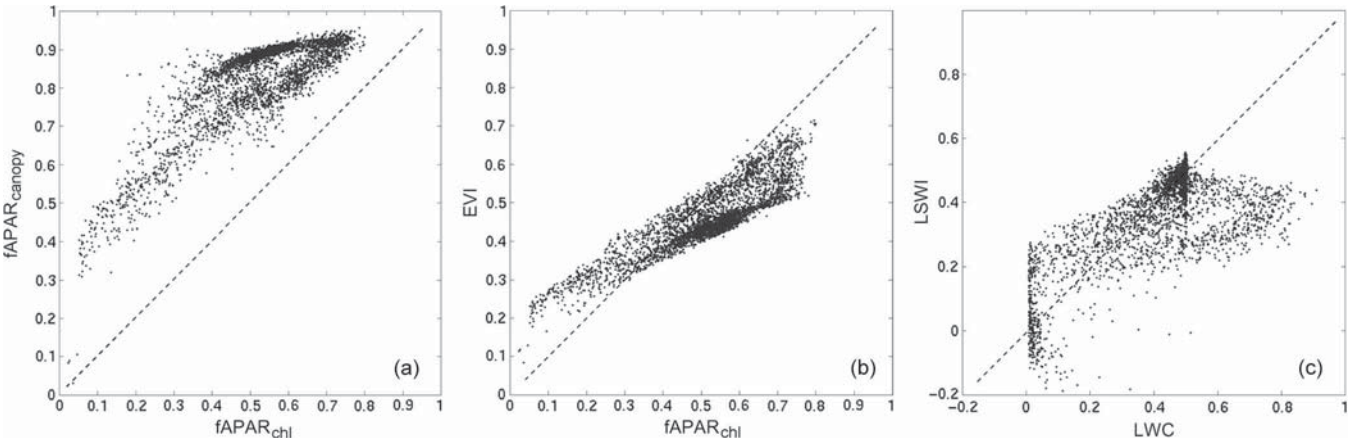

Fig. 7. Comparisons for (a) $\mathrm{fAPAR_{chl}}$ versus $\mathrm{fAPAR_{canopy}}$, (b) $\mathrm{fAPAR_{chl}}$ versus EVI, and (c) LWC versus LSWI. Data are derived from the simulated HyspIRI image acquired on DOY 180, 2008 (June 28, 2008).

TABLE III
COMPARISON AT THE DF49 TOWER SITE OF THE $fAPAR_{chl}$, $fAPAR_{canopy}$, NDVI, EVI, LSWI, AND LWC VALUES FROM THE SIMULATED HYSPIRI-LIKE (60 m) IMAGE WITH THE MODIS IMAGE (500 m) AND PUBLISHED FIELD MEASUREMENTS (H: HYSPIRI-LIKE DATA; M: SEVEN-BAND MODIS-BASED DATA)

	Parameters		Value (± STDEV)	Sample size, Comments
fAPAR related parameters	$fAPAR_{chl}$	H	0.583 ± 0.038	n = 49 pixels
		M	0.533	single pixel value
	$fAPAR_{canopy}$	H	0.907 ± 0.006	n = 49 pixels
		M	0.949	single pixel value
		Tower based	0.94	Hember et al. [29] day 180-185 of 2008
	NDVI	H	0.867 ± 0.005	n = 49 pixels
		M	0.901	single pixel value
	EVI	H	0.449 ±0.017	n = 49 pixels
		M	0.445	single pixel value
	$fAPAR_{green-leaf}$	Tower based	0.79	Hilker et al. [30] day 180-185 of 2008
Leaf water related parameters	LWC	H	0.494 ± 0.008	n = 49 pixels
		M	0.493	single pixel value
		Field measurements	0.44 – 0.67	Agee et al. [33], Keyes [34] growing season of multiyears
	LSWI	H	0.506 ± 0.013	n = 49 pixels
		M	0.510	single pixel value

for $fAPAR_{chl}$ values [Fig. 5(a) and (b)]. When comparing $fAPAR_{chl}$ and EVI, we found that, when $fAPAR_{chl} = 0.5$, the EVI range is 0.384–0.533, but when EVI $= 0.5$, the $fAPAR_{chl}$ range is 0.410–0.686 [Fig. 7(b)].

In addition to better spatial detail, one advantage of the seven-band $fAPAR_{chl}$ and LWC algorithm is that it does not need land cover type information as an input to run the model inversion, whereas the MODIS standard $fAPAR_{canopy}$ (i.e., FPAR) product does. The seven-band algorithm can provide $fAPAR_{chl}$ and LWC products with less uncertainty (e.g., smaller standard deviations) as compared to results obtained with the previous five-band algorithm, even for a relatively homogeneous forest area [circle in Fig. 1(b)]. The outputs of the algorithm ($fAPAR_{chl}$ and LWC) can be used for seasonal analysis, interannual analysis, phenological study, and land use and land cover change research—including disturbance studies and disaster monitoring (e.g., fire, drought, and flooding). Our study also demonstrates the flexibility that an imaging spectrometer allows for interinstrument comparisons.

The remote sensing community uses three groups of inversion strategies: MCMC approaches, look-up tables, and gradient-based approaches. With the Metropolis approach (an MCMC method), we can globally search for the optimal solution, a posterior distribution. However, look-up-table methods provide fixed step lengths for all parameters before inversion, whereas gradient-based methods can only search local optima and rely on initial guesses. We anticipate that application of our algorithm to satellite images will be useful for the current and future national and international research projects that rely on remotely sensed data, including the North American Carbon Program.

V. CONCLUSION

We have successfully demonstrated here that the two products ($fAPAR_{chl}$ and LWC) provide unique information. The most important finding in this paper is that $fAPAR_{chl}$ values differ from those for EVI, NDVI, and $fAPAR_{canopy}$ in most cases. EVI is not always equal to $fAPAR_{chl}$. We have also found the following: $fAPAR_{chl} \neq fAPAR_{canopy}$ (or NDVI), and LWC $\neq$ LSWI. In other words, we have rejected the null hypotheses that equate the EVI and $fAPAR_{canopy}$ with $fAPAR_{chl}$ or LSWI with LWC. HyspIRI also has the potential to provide the spatial variance of the two products that cannot be extracted from MODIS. We have realized that real HyspIRI images, or those of another future imaging spectrometer, will differ in some ways from Hyperion, which can be taken into account with the at-launch version of the algorithm.

APPENDIX

In brief, a vegetation canopy can be partitioned into leaf and nonleaf (hereafter referred to as stem) components. A leaf can be further partitioned into chlorophyll, nonphotosynthetic pigments (hereafter referred to as brown pigment C_{brown}), water, and dry matter (or C_{ab}, C_{brown}, C_w, and C_m). The PROSAIL2 model has 14 biophysical and biochemical variables: plant area index, stem fraction (SFRAC), cover fraction, stem inclination angle (STINC), stem BRDF effect variable (STHOT), leaf inclination angle (LFINC), leaf BRDF effect variable (LFHOT), five leaf variables that simulate leaf optical properties (N, C_{ab}, C_m, C_w, and C_{brown}), one soil/litter variable that simulates soil/litter optical properties $(SOIL_A)$, and one variable that simulates stem optical properties $(STEM_A)$. The MCMC method (Methopolis) is employed for inversion.

One can calculate $fAPAR_{canopy}$ [12] and $fAPAR_{chl}$ [11] with

$$APAR_{\text{canopy}} = APAR_{\text{chl}} + APAR_{\text{dry matter}} + APAR_{\text{brown pigment}} + APAR_{\text{stem}} \quad \text{(A1)}$$

$$fAPAR_{\text{canopy}} = \frac{APAR_{\text{canopy}}}{PAR_0} \quad \text{(A2)}$$

$$fAPAR_{\text{chl}} = \frac{APAR_{\text{chl}}}{PAR_0} \quad \text{(A3)}$$

where PAR_0 is the incoming PAR at the top of the canopy and $APAR_{canopy}$, $APAR_{chl}$, $APAR_{dry\ matter}$, $APAR_{brown\ pigment}$, and $APAR_{stem}$ are PAR absorbed by canopy, chlorophyll in leaf, dry matter in leaf, brown pigment in leaf, and stem, respectively. One has to know the value of PAR_0 and the values of the 14 parameters to calculate $APAR_{chl}$ and $APAR_{canopy}$ in (A1). One may assume PAR_0 be any positive value to calculate $fAPAR_{chl}$ and $fAPAR_{canopy}$ because they are ratios [(A2) and (A3)]. We present NDVI-based $fAPAR_{canopy}$ for this paper because of the linear relationship between $fAPAR_{canopy}$ and NDVI (3), which is based on the simulation study using the SAIL [12].

The leaf water thickness (C_w in grams per square centimeter or centimeter) and leaf dry matter (C_m in grams per square centimeter) are two of the 14 parameters of PROSAIL2, and the inversion algorithm provides their posterior distributions as outputs. LWC is defined as the fraction of leaf water weight to fresh leaf weight [35]. That is to say

$$LWC = \frac{C_W}{C_W + C_m}. \tag{A4}$$

EVI [25], NDVI [26], and LSWI [14] are also calculated:

$$EVI = 2.5 \times \frac{\rho_{\mathrm{NIR}_1} - \rho_{\mathrm{red}}}{\rho_{\mathrm{NIR}_1} + 6.0 \times \rho_{\mathrm{red}} - 7.5 \times \rho_{\mathrm{blue}} + 1.0} \tag{A5}$$

$$NDVI = \frac{\rho_{\mathrm{NIR}_1} - \rho_{\mathrm{red}}}{\rho_{\mathrm{NIR}_1} + \rho_{\mathrm{red}}} \tag{A6}$$

$$LSWI = \frac{\rho_{\mathrm{NIR}_1} - \rho_{\mathrm{SWIR}_1}}{\rho_{\mathrm{SWIR}_1} + \rho_{\mathrm{SWIR}_1}} \tag{A7}$$

where ρ is the reflectance.

ACKNOWLEDGMENT

The authors would like to thank the four anonymous reviewers who have provided helpful suggestion and comments for this paper.

REFERENCES

[1] J. S. Kimball, L. A. Jones, K. Zhang, F. A. Heinsch, K. C. McDonald, and W. C. Oechel, "A satellite approach to estimate land–atmosphere CO_2 exchange for boreal and arctic biomes using MODIS and AMSR-E," *IEEE Trans. Geosci. Remote Sens.*, vol. 47, no. 2, pp. 569–587, Feb. 2009.

[2] X. Xiao, "Light absorption by leaf chlorophyll and maximum light use efficiency," *IEEE Trans. Geosci. Remote Sens.*, vol. 44, no. 7, pp. 1933–1935, Jul. 2006.

[3] F. A. Heinsch, M. Zhao, S. W. Running, J. S. Kimball, R. R. Nemani, K. J. Davis, P. V. Bolstad, B. D. Cook, A. R. Desai, D. M. Ricciuto, B. E. Law, W. C. Oechel, H. Kwon, H. Luo, S. C. Wofsy, A. L. Dunn, J. W. Munger, D. D. Baldocchi, L. Xu, D. Y. Hollinger, A. D. Richardson, P. C. Stoy, M. B. S. Siqueira, R. K. Monson, S. P. Burns, and L. B. Flanagan, "Evaluation of remote sensing based terrestrial productivity from MODIS using regional tower eddy flux network observations," *IEEE Trans. Geosci. Remote Sens.*, vol. 44, no. 7, pp. 1908–1925, Jul. 2006.

[4] P. J. Sellers, D. A. Randall, G. J. Collatz, J. A. Berry, C. B. Field, D. A. Dazlich, C. Zhang, G. D. Collelo, and L. Bounoua, "A revised land surface parameterization (SiB2) for atmospheric GCMs.I: Model formulation," *J. Climate*, vol. 9, no. 4, pp. 676–705, Apr. 1996.

[5] R. H. Waring, N. C. Coops, and J. J. Landsberg, "Improving predictions of forest growth using the 3-PGS model with observations made by remote sensing," *Forest Ecol. Manag.*, vol. 259, no. 9, pp. 1722–1729, Apr. 2010.

[6] P. J. Sellers, S. O. Los, C. J. Tucker, C. O. Justice, D. A. Dazlich, G. J. Collatz, and D. A. Randall, "A revised land surface parameterization (SiB2) for atmospheric GCMs.II: The generation of global fields of terrestrial biophysical parameters from satellite data," *J. Climate*, vol. 9, no. 4, pp. 706–737, Apr. 1996.

[7] R. E. Dickinson, "Applications of terrestrial remote sensing to climate modeling," in *Advances Land Remote Sensing*, S. Liang, Ed. New York: Springer-Verlag, 2008.

[8] D. P. Turner, W. D. Ritts, W. B. Cohen, S. T. Gower, M. S. Zhao, S. W. Running, S. C. Wofsy, S. Urbanski, A. L. Dunn, and J. W. Munger, "Scaling gross primary production (GPP) over boreal and deciduous forest landscapes support of MODIS GPP product validation," *Remote Sens. Environ.*, vol. 88, no. 3, pp. 256–270, Dec. 15, 2003.

[9] D. P. Turner, S. Urbanski, D. Bremer, S. C. Wofsy, T. Meyers, S. T. Gower, and M. Gregory, "A cross-biome comparison of daily light use efficiency for gross primary production," *Global Change Biol.*, vol. 9, no. 3, pp. 383–395, Mar. 2003.

[10] D. P. Turner, W. D. Ritts, M. Zhao, S. A. Kurc, A. L. Dunn, S. Wofsy, E. Small, and S. W. Running, "Assessing interannual variation MODIS-based estimates of gross primary production," *IEEE Comput. Sci. Eng.*, vol. 44, no. 7, pp. 1899–1907, Jul. 2006.

[11] Q. Zhang, E. M. Middleton, H. A. Margolis, G. G. Drolet, A. A. Barr, and T. A. Black, "Can a MODIS-derived estimate of the fraction of PAR absorbed by chlorophyll (FAPARchl) improve predictions of light-use efficiency and ecosystem photosynthesis for a boreal aspen forest?," *Remote Sens. Environ.*, vol. 113, no. 4, pp. 880–888, Apr. 15, 2009.

[12] S. N. Goward and K. F. Huemmrich, "Vegetation canopy PAR absorptance and the normalized difference vegetation index—An assessment using the SAIL model," *Remote Sens. Environ.*, vol. 39, no. 2, pp. 119–140, Feb. 1992.

[13] D. A. Sims, A. F. Rahman, V. D. Cordova, D. D. Baldocchi, L. B. Flanagan, A. H. Goldstein, D. Y. Hollinger, L. Misson, R. K. Monson, H. P. Schmid, S. C. Wofsy, and L. K. Xu, "Midday values of gross CO_2 flux and light use efficiency during satellite overpasses can be used to directly estimate eight-day mean flux," *Agric. Forest Meteorol.*, vol. 131, no. 1/2, pp. 1–12, Jul. 2005.

[14] X. M. Xiao, Q. Y. Zhang, B. Braswell, S. Urbanski, S. Boles, S. Wofsy, B. Moore, and D. Ojima, "Modeling gross primary production of temperate deciduous broadleaf forest using satellite images and climate data," *Remote Sens. Environ.*, vol. 91, no. 2, pp. 256–270, May 30, 2004.

[15] C. O. Justice, E. Vermote, J. R. G. Townshend, R. Defries, D. P. Roy, D. K. Hall, V. V. Salomonson, J. L. Privette, G. Riggs, A. Strahler, W. Lucht, R. B. Myneni, Y. Knyazikhin, S. W. Running, R. R. Nemani, Z. M. Wan, A. R. Huete, W. van Leeuwen, R. E. Wolfe, L. Giglio, J. P. Muller, P. Lewis, and M. J. Barnsley, "The MODerate resolution Imaging Spectroradiometer (MODIS): Land remote sensing for global change research," *IEEE Trans. Geosci. Remote Sens.*, vol. 36, no. 4, pp. 1228–1249, Jul. 1998.

[16] B. D. Cook, P. V. Bolstad, E. Næsset, R. S. Anderson, S. Garrigues, J. T. Morisette, J. Nickeson, and K. J. Davis, "Using LiDAR and QuickBird data to model plant production and quantify uncertainties associated with wetland detection and land cover generalizations," *Remote Sens. Environ.*, vol. 113, no. 11, pp. 2366–2379, Nov. 2009.

[17] X. M. Xiao, Q. Y. Zhang, S. Saleska, L. Hutyra, P. D. Camargo, S. Wofsy, S. Frolking, S. Boles, M. Keller, and M. B. , "Satellite-based modeling of gross primary production a seasonally moist tropical evergreen forest," *Remote Sens. Environ.*, vol. 94, no. 1, pp. 105–122, Jan. 2005.

[18] Y. J. Kaufman and D. Tanre, "Strategy for direct and indirect methods for correcting the aerosol effect on remote sensing: From AVHRR to EOS-MODIS," *Remote Sens. Environ.*, vol. 55, no. 1, pp. 65–79, Jan. 1996.

[19] B.-C. Gao, K. H. Heidebrecht, and A. F. H. Goetz, "Derivation of scaled surface reflectances from AVIRIS data," *Remote Sens. Environ.*, vol. 44, no. 2/3, pp. 165–178, Jun. 1993.

[20] B.-C. Gao and C. O. Davis, "Development of a line-by-line-based atmosphere removal algorithm for airborne and spaceborne imaging spectrometers," *SPIE*, vol. 3118, pp. 132–141, 1997.

[21] E. F. Vermote, D. Tanre, J. L. Deuze, M. Herman, and J. J. Morcrette, "Second simulation of the satellite signal the solar spectrum, 6S: An overview," *IEEE Trans. Geosci. Remote Sens.*, vol. 35, no. 3, pp. 675–686, May 1997.

[22] S. G. Ungar, J. S. Pearlman, J. A. Mendenhall, and D. Reuter, "Overview of the Earth Observing One (EO-1) mission," *IEEE Trans. Geosci. Remote Sens.*, vol. 41, no. 6, pp. 1149–1159, Jun. 2003.

[23] X. Hao and J. J. Qu, "Retrieval of real-time live fuel moisture content using MODIS measurements," *Remote Sens. Environ.*, vol. 108, no. 2, pp. 130–137, May 2007.

[24] Q. Y. Zhang, X. M. Xiao, B. Braswell, E. Linder, F. Baret, and B. Moore, "Estimating light absorption by chlorophyll, leaf and canopy a deciduous broadleaf forest using MODIS data and a radiative transfer model," *Remote Sens. Environ.*, vol. 99, no. 3, pp. 357–371, Nov. 2005.
[25] A. R. Huete, H. Q. Liu, K. Batchily, and W. vanLeeuwen, "A comparison of vegetation indices global set of TM images for EOS-MODIS," *Remote Sens. Environ.*, vol. 59, no. 3, pp. 440–451, Mar. 1997.
[26] D. W. Deering, *Rangeland Reflectance Characteristics Measured by Aircraft and Spacecraft Sensors*. College Station, TX: Texas A&M Univ., 1978, p. 338.
[27] T. Hilker, N. C. Coops, C. R. Schwalm, R. S. Jassal, T. A. Black, and P. Krishnan, "Effects of mutual shading of tree crowns on prediction of photosynthetic light-use efficiency a coastal Douglas-fir forest," *Tree Physiol.*, vol. 28, no. 6, pp. 825–834, Jun. 2008.
[28] Q. Zhang, X. Xiao, B. Braswell, E. Linder, S. Ollinger, M. L. Smith, J. P. Jenkins, F. Baret, A. D. Richardson, B. Moore, and R. Minocha, "Characterization of seasonal variation of forest canopy a temperate deciduous broadleaf forest, using daily MODIS data," *Remote Sens. Environ.*, vol. 105, no. 3, pp. 189–203, Dec. 2006.
[29] R. A. Hember, N. C. Coops, T. A. Black, and R. D. Guy, "Simulating gross primary production across a chronosequence of coastal Douglas-fir forest stands with a production efficiency model," *Agric. Forest Meteorol.*, vol. 150, no. 2, pp. 238–253, Feb. 2010.
[30] T. Hilker, F. G. Hall, N. C. Coops, A. Lyapustin, Y. Wang, Z. Nesic, N. Grant, T. A. Black, M. A. Wulder, N. Kljun, C. Hopkinson, and L. Chasmer, "Remote sensing of photosynthetic light-use efficiency across two forested biomes: Spatial scaling," *Remote Sens. Environ.*, vol. 114, no. 12, pp. 2863–2874, Dec. 2010.
[31] J. M. Chen, "Canopy architecture and remote sensing of the fraction of photosynthetically active radiation absorbed by boreal conifer forests," *IEEE Trans. Geosci. Remote Sens.*, vol. 34, no. 6, pp. 1353–1368, Nov. 1996.
[32] J. M. Chen, A. Govind, O. Sonnentag, Y. Zhang, A. Barr, and B. Amiro, "Leaf area index measurements at Fluxnet-Canada forest sites," *Agric. Forest Meteorol.*, vol. 140, no. 1–4, pp. 257–268, Nov. 2006.
[33] J. K. Agee, C. S. Wright, N. Williamson, and M. H. Huff, "Foliar moisture content of Pacific Northwest vegetation and its relation to wildland fire behavior," *Forest Ecol. Manag.*, vol. 167, no. 1–3, pp. 57–66, Aug. 2002.
[34] C. R. Keyes, "Foliar moisture contents of North American conifers," *USDA Forest Service Proc.*, vol. RMRS-41, pp. 395–399, 2006.
[35] E. Garnier and G. Laurent, "Leaf anatomy, specific mass and water content congeneric annual and perennial grass species," *New Phytologist*, vol. 128, no. 4, pp. 725–736, Dec. 1994.

Qingyuan Zhang received the B.S. degree in mathematics from Shandong University, Jinan, China, in 1994, the M.S. degree in applied mathematics from Tsinghua University, Beijing, China, in 1996, and the Ph.D. degree in natural resources and environmental studies from the University of New Hampshire, Durham, in 2006.

From 1996 to 1998, he was a Research Scientist with the Institute of Remote Sensing Applications, Chinese Academy of Sciences, Beijing. From 1999 to 2000, he was a Visiting Research Scientist with the Earth Observation Research Center, National Space Development Agency of Japan, Tokyo, Japan. In July 2006, he joined the Goddard Space Flight Center through a cooperative agreement with the University of Maryland, Baltimore County. He is currently with the Goddard Space Flight Center and Universities Space Research Association, Columbia, MD. His recent research interests include retrieving vegetation parameters through inversion of remote sensing models, multisensor data fusion, remote sensing of biogeochemical cycling and ecosystems, global carbon cycling, and global change.

Dr. Zhang received the Outstanding Student Paper Awards in 2004 and 2005 Fall AGU. He received an Honorary Certificate of Beijing Municipal Science and Technology Prize from Beijing Municipal People's Government, China, in February 2005. He also received the TECH BRIEF INITIAL AWARD from NASA on May 18, 2010.

Elizabeth M. Middleton (M'95) received the B.S. degree in zoology, the M.S. degree in ecology, and the Ph.D. degree in botany from the University of Maryland, College Park, in 1967, 1976, and 1993, respectively.

She is a Senior Scientist with the Laboratory for Biospheric Sciences (new Code 618), NASA Goddard Space Flight Center (GSFC), Greenbelt, MD. She is currently the Mission Scientist for the Earth Exploring One (EO-1) satellite and the GSFC lead for the NASA HyspIRI satellite concept development. She has previously served, and is currently serving, as the Outside Observer on the Mission Advisory Group (2007–2009 and 2011+) for a European Space Agency Phase A satellite mission concept—the Fluorescence Explorer. In addition, she was a member of the NASA/GSFC Carbon Cycle Science Working Group (2000–2007) and the NASA representative to the U.S. Federal Geographic Data Committee's Vegetation Subcommittee for many years. She leads a research team that studies vegetation spectral bioindicators of plant stress and photosynthetic function, including plant fluorescence. She is an Associate Editor of the *Journal of Applied Remote Sensing*.

Dr. Middleton recently received a Career Achievement Award from the Hydrospheric and Biospheric Sciences Laboratory, GSFC, in 2011. She also received the NASA Group Achievement Awards in 1983, 1994, 1995, and 2003, in addition to numerous performance awards.

Bo-Cai Gao received the B.S. degree in physics from Nankai University, Tianjin, China, in 1982 and the M.S. and Ph. D degrees in physics from The Ohio State University, Columbus, in 1984 and 1988, respectively.

He is currently with the Remote Sensing Division, Naval Research Laboratory, Washington, DC. He has conducted research on remote sensing of cirrus clouds, atmospheric water vapor, and coastal water using multichannel data collected with the NASA Terra and Aqua MODIS instruments. He is the inventor of the Normalized Difference Water Index, which is widely used in the vegetation research community.

Dr. Gao received a Prize Paper Award from the IEEE Geoscience and Remote Sensing Society in 1991 for his development of an operational atmospheric radiative transfer code to retrieve surface reflectance spectra from hyperspectral imaging data measured with the NASA/JPL Airborne Visible/Infrared Imaging Spectrometer.

Yen-Ben Cheng received the B.S. and M.S. degrees in agricultural engineering from National Taiwan University, Taipei, Taiwan, in 1996 and 1998, respectively, and the Ph.D. degree in hydrologic sciences from the University of California, Davis, in 2006.

He is currently a Research Scientist with Earth Resources Technology, Inc., Annapolis Junction, MD, working for the NASA Goddard Space Flight Center. His research interests include accurate retrievals of leaf biochemical and canopy biophysical properties, and land surface parameterization for ecological and hydrological applications.